



Rapporti Tecnici INAF INAF Technical Reports

Number	210
Publication Year	2022
Acceptance in OA@INAF	2022-12-15T10:44:35Z
Title	BC-SIM-TN-013 STC Inflight Dark Calibration
Authors	SIMIONI, Emanuele; Da Deppo, Vania; ZUSI, MICHELE; BALESTRA, Andrea; POLITI, ROMOLO; DELLA CORTE, VINCENZO; SLEMER, Alessandra; CREMONESE, Gabriele; CAPACCIONI, FABRIZIO; RE, Cristina; Doressoundiram, Alain; PALUMBO, PASQUALE; Vincendon, Mathieu
Affiliation of first author	O.A. Padova
Handle	http://hdl.handle.net/20.500.12386/32746 ; https://doi.org/10.20371/INAF/TechRep/210

BC-SIM-TN-013

STC Inflight Dark Calibration

Emanuele Simioni¹, Vania Da Deppo², Michele Zusi³, Andrea Balestra¹
Romolo Politi³, Vincenzo della Corte³, Alessandra Slemer⁴
Gabriele Cremonese¹, Fabrizio Capaccioni³, Cristina Re¹, Alain Doressoundiram⁵,
Pasquale Palumbo⁷, Mathieu Vincendon⁶

¹INAF-Osservatorio Astronomico di Padova, Vicolo Osservatorio 5,35122, Padua, Italy

²CNR-IFN, via Trasea, 7, 35131, 00133, Padova, Italy

³INAF- Istituto Astrofisica e Planetologia Spaziali, Via Fosso del Cavaliere 100, 00133, Rome, Italy

⁴Officina Stellare S.p.A., via della tecnica 87/89, 36060 Sarcedo (VI)

⁵Observatoire de Paris - PSL, Laboratoire d'Études Spatiales et d'Instrumentation en Astrophysique (LESIA), 92195 Meudon Cedex, France

⁶Institut d'Astrophysique Spatiale, CNRS / Université Paris Sud, 91405, Orsay, France

⁷Università Parthenope, Centro Direzionale Isola 4, 80133, Naples, Italy

Index

INDEX	1
1. INTRODUCTION	4
1.1. SCOPE	4
1.2. REFERENCE DOCUMENTS	5
1.2.1. <i>Documentations</i>	5
1.2.2. <i>Publications</i>	6
1.3. ACRONYMS	7
1.1. DOCUMENT FORMAT AND REPOSITORY	7
1.4. DOCUMENT ORGANIZATION	8
2. INSTRUMENT CONTEXT	1
2.1. STC STEREO CAMERA	2
2.1.1. <i>Optical Design and purpose</i>	2
2.1.2. <i>STC Detector</i>	4
2.2. STC ON GROUND CALIBRATION	6
<i>Optical calibration</i>	6
<i>Dark Calibration</i>	6
2.2.1. <i>Volcano Issue</i>	8
2.2.2. <i>Reset Issue</i>	9
2.2.2.1. <i>Reset Issue Solution</i>	11
<i>Offset Dark Subtraction</i>	11
<i>Mitigation</i>	12
2.3. OPERATION ACTIVITIES: FLIGHT OPERATION PROCEDURE	13
3. CHECK OUTS TIMELINES	15
3.1. NECP AND DNECP PHASE	16
3.2. ICO1 PHASE	17
3.2.1. <i>Functional Test</i>	17
3.2.2. <i>Performance Test Planning</i>	18
3.2.2.1. <i>Performance Test Analysis</i>	18
3.2.3. <i>ICO1 Results</i>	22
3.3. ICO2 PHASE	23
3.3.1. <i>Test Planning</i>	23
3.3.2. <i>Test analysis</i>	23
3.3.3. <i>ICO Results</i>	26
3.4. ICO3 PHASE	27

3.4.1.	<i>Test Planning</i>	27
3.4.2.	<i>Low IT (0.288 ms) Analysis</i>	28
3.4.3.	<i>Higher IT (9.6 ms) Analysis</i>	28
3.4.4.	<i>ICO3 phase: GM analysis</i>	29
3.4.5.	<i>ICO3 phase: CM analysis</i>	31
3.4.6.	<i>ICO3 Results</i>	31
3.5.	ICO4 PHASE	33
3.5.1.	<i>GM with max RT</i>	33
3.5.2.	<i>Mitigate test</i>	37
3.5.3.	<i>ICO4 Results</i>	38
4.	CONCLUSIONS	39
4.1.	GLOBAL MAPPING	39
4.2.	COLOR MODE	39

Approval

Edited by:	E.Simioni
Revised by:	Vincenzo della Corte
	Michele Zusi
	Gianrico Filacchione
	Cristina Re
	Vania Da Deppo
Approved by:	G. Cremonese

Document Change Record

Issue	Revision	Date	Affected Pages	Change description
1	0	03/07/2022	All	First Release

1. Introduction

1.1.Scope

In this document, we reported the history of the tests performed on the STC detector in the first two years of the BepiColombo's cruise phase. The scope of these tests was to monitor the dark current behavior of the STC channel's detector. A detailed description is provided for each test phase: data acquired, the deducted results and conclusions.

The STC Channel is part of SIMBIO-SYS, a scientific payload of the BepiColombo ESA-JAXA mission to Mercury.

During the NECP (Near-Earth Commissioning Phase), all the initial commissioning activities were completed and the three channels of SIMBIO-SYS have operated properly demonstrating that all the channels and subsystems worked nominally.

Since then, every six months different instrument checkouts have been carried-out to check the performance of the three SIMBIO-SYS channels and improve their calibration.

This document reports the conclusion on the Dark calibration of STC Channel due to the analysis of the ICOs tests.

1.2. Reference Documents

1.2.1. Documentations

- [RD.1] BC-SIM-TN-003 Reports and Note Layout and Flow (10.20371/INAF/TechRep/36)
- [RD.2] BC-SIM-TN-002_-_STC_Strategy_Observation (10.20371/INAF/TechRep/35)
- [RD.3] BC-SIM-PI-RP-001- SIMBIO-SYS INSTRUMENT SCIENCE PERFORMANCE REPORT
- [RD.4] BC-SIM-TN-001_-_The_Flight_Operation_Procedures_of_the_SIMBIO-SYS_instrument_ aboard_the_BepiColombo_ESA_mission 10.20371/INAF/TechRep/15
- [RD.5] BC-SIM-TN-004_-_SIMBIO-SYS_FOP_update_after_NECPhhttp: 10.20371/INAF/TechRep/58
- [RD.6] BC-SIM-TN-008_-_SIMBIO-SYS_FOP_update_after_ICO#02 10.20371/INAF/TechRep/162
- [RD.7] BC-SIM-TR-003_-_STC_NECP_report 10.20371/INAF/TechRep/26
- [RD.8] BC-SIM-TR-007_-_STC_dNECP_report 10.20371/INAF/TechRep/71
- [RD.9] BC-SIM-TR-013_-_STC_ICO#01_report 10.20371/INAF/TechRep/89
- [RD.10] BC-SIM-TR-019_-_STC_ICO#02_report 10.20371/INAF/TechRep/138
- [RD.11] BC-SIM-TR-XXX_-_STC_ICO#03_report (10.20371/INAF/TechRep/186)
- [RD.12] BC-SIM-TR-XXX_-_STC_ICO#04_report 10.20371/INAF/TechRep/208

1.2.2. Publications

- [RD.14] Cremonese G., et al. (2009) , "The stereo camera on the BepiColombo ESA/JAXA mission: a novel approach", *Advances in Geosciences*, 15, 305. [10.1142/9789812836229_0019](https://doi.org/10.1142/9789812836229_0019)
- [RD.15] F. Capaccioni et al. (2009), "The visible and infrared hyperspectral imager (VIHI) of the BepiColombo MPO mission: development status and observation strategy", *GRA* , Vol.11, EGU2009-12214, [10.1109/TGRS.2010.2051676](https://doi.org/10.1109/TGRS.2010.2051676)
- [RD.16] L. Colangeli, et al., "The High Resolution Imaging Channel of the SIMBIO-SYS instrument on board the BepiColombo mission to Mercury", 37th COSPAR Scientific Assembly, vol. 37. 2008.
- [RD.17] Zusi, M., et al (2019). "Optical design of the high resolution imaging channel of SIMBIO-SYS". *Applied optics*, 58(15), 4059-4069.
- [RD.18] Cremonese, G et al., (2020). "SIMBIO-SYS: Scientific Cameras and Spectrometer for the BepiColombo Mission". *Space Science Reviews*, 216(5), 1-78. [10.1007/s11214-020-00704-8](https://doi.org/10.1007/s11214-020-00704-8)
- [RD.19] Benkhoff, J., et al (2010). "BepiColombo—Comprehensive exploration of Mercury: Mission overview and science goals". *Planetary and Space Science*, 58(1-2), 2-20. [10.1016/j.pss.2009.09.020](https://doi.org/10.1016/j.pss.2009.09.020)
- [RD.20] Da Deppo et al. (2006) "Preliminary optical design of the stereo channel of the imaging system SIMBIOSYS for the Bepicolombo ESa mission" *ICSO* , ESTEC, Noordwijk, ESA SP-621, June 006
- [RD.21] Simioni, E., et al. (2019). "SIMBIO-SYS/STC stereo camera calibration: Geometrical distortion". *Review of Scientific Instruments*, 90(4), 043106. [10.1063/1.5085710](https://doi.org/10.1063/1.5085710)
- [RD.22] Slemmer, A., et al. (2020) "Development of a simulator of the SIMBIOSYS suite onboard the BepiColombo mission". *Monthly Notices of the Royal Astronomical Society*, 491.2: 1673-1689.
- [RD.23] R. E. Mills, et al. (2009) "Advanced staring Si PIN visible sensor chip assembly for Bepi-Colombo mission to Mercury", *Proc. SPIE*, vol. 7439, 74390A, 2009.
- [RD.24] Thomas, N., et al (2017). "The colour and stereo surface imaging system (CaSSIS) for the ExoMars trace gas orbiter. *Space science reviews*," 212(3-4), 1897-1944. [10.1007/s11214-017-0421-1](https://doi.org/10.1007/s11214-017-0421-1)
- [RD.25] Da Deppo, et al. (2014). "Characterization of the integrating sphere for the on-ground calibration of the SIMBIOSYS instrument for the BepiColombo ESA mission". In *Space Telescopes and Instrumentation 2014* (Vol. 9143, p. 914344). International Society for Optics and Photonics. [10.1117/12.2057349](https://doi.org/10.1117/12.2057349)
- [RD.26] Simioni, E., et al. (2021). 3dpp: A Photogrammetric Pipeline For A Push Frame Stereo Cameras. *Planetary and Space Science*, 105165. (2021) [10.1016/j.pss.2021.105165](https://doi.org/10.1016/j.pss.2021.105165)
- [RD.27] Slemmer, A., et al., (2019). "Radiometric calibration of the SIMBIO-SYS STereo imaging Channel". *CEAS Space Journal*, 11(4), 485-496. [10.1007/s12567-019-00277-5](https://doi.org/10.1007/s12567-019-00277-5)
- [RD.28] Coope, Ian D. "Circle fitting by linear and nonlinear least squares." *Journal of Optimization Theory and Applications* 76.2 (1993): 381-388. [10.1007/BF00939613](https://doi.org/10.1007/BF00939613)
- [RD.29] Acton JR, et al. (1996) "Ancillary data services of NASA's navigation and ancillary information facility". *Planetary and Space Science*, 44.1: 65-70.
- [RD.30] Re, C., et al. (2017). "Effects of image compression and illumination on digital terrain models for the stereo camera of the BepiColombo mission". *Planetary and Space Science*, 136, 1-14.
- [RD.31] Simioni, E., et al. (2019). SIMBIOSYS-STC ready for launch: a technical recap. In *International Conference on Space Optics—ICSO 2018* (Vol. 11180, p. 1118042). International Society for Optics and Photonics.
- [RD.32] Simioni, E., et al. (2017). CMOS detectors: lessons learned during the STC stereo channel preflight calibration. In *International Conference on Space Optics—ICSO 2016* (Vol. 10562, p. 105622M).
- [RD.33] SIMMS, Lance Michael (2010). "Hybrid CMOS SiPIN detectors as astronomical imagers". Stanford University.
- [RD.34] Zusi, M., et al. "SIMBIO-SYS Near Earth Commissioning Phase: a step forward toward Mercury". In: *Infrared Remote Sensing and Instrumentation XXVII*. International Society for Optics and Photonics, 2019. p. 111280V.

[RD.35] Xuli Han et al (2018), "Cubic Hermite interpolation with minimal derivative oscillation", Journal of Computational and Applied Mathematics, Volume 331, Pages 82-87,ISSN 0377-0427, [10.1016/j.cam.2017.09.049](https://doi.org/10.1016/j.cam.2017.09.049).

1.3.Acronyms

APID	Application Process Identifier
CSV	Comma Separated Values
FOP	Flight Operation Plan.
FPA	Focal Plane Assembly
HK	Housekeeping
HRIC	High spatial Resolution Imaging Channel
ME	Main Electronics
NECP	Near Earth Commissioning Phase
ODS	Offset Dark Subtraction
PDS	Planetary Data System
PDOR	Payload Direct Operation Request
PE	Proximity Electronics
PNG	Portable Network Graphics
PSC	Packet Sequence Control
SIMBIO-SYS	Spectrometers and Imagers for MPO BepiColombo Integrated Observatory SYStem
SSC	Source Sequence Count
STC	STereo imaging Channel
TC	Telecommand
TM	Telemetry
VIHI	VIsible and Hyper-spectral Imaging channel
XML	eXtensible Markup Language

1.1. Document Format and Repository

This document is compliant with the SIMBIO-SYS Report and Note Layout and Flow [RD.1] and will be archived both on the INAF Open Access repository and the SIMBIO-SYS team Archive.

1.4. Document organization

In this paper, we focus our analysis on the dark response characterization of the STC channel performed in the first two years of the BepiColombo journey. These measurements allowed us to clarify all the open issues inherited from the on-ground calibration and demonstrate the correct strategy for a detailed calibration of the instrument dark.

This paper is organized in several sections addressing specific arguments: the context of STC instrument is described in Section 2.1 with a detailed subsection about the detector, the goal of most of the investigations described.

Section 2.2 details an overview of the calibration activities performed on ground underling the calibration issues identified during the onground calibration more investigated in the inflight ICOs.

Section 2.3 details the operation activities developed to approach the SIMBIO-SYS Instrument Check Outs (ICO). The different phases are reported in Section 3 and described in the subsequent Sections (see **Table 1**) which report for each ICO purposes and results.

Phase	Hyperlinks	
	Section	Page
NECP	3.1	16
DNECP	3.1	16
ICO1	3.2	17
ICO2	3.3	23
ICO3	3.4	27
ICO4	3.5	33

Table 1 Table of the sections describing the different in flight test phase

Each Section will report a final subsection with the results and the conclusion of the analysis.

Section 4 reports the conclusions.



BepiColombo SIMBIO-SYS

Reference: BC-SIM-TN-013-STC Inflight
DarkError! **Unknown**
document property name.

Issue : 1

Rev. : 1

Date: 03/07/2020

Page: 9

2. INSTRUMENT CONTEXT

STC (Stereo Imaging Channel) ([RD.14]) together with VIHI (Visual and near-Infrared Hyper-spectral Imaging channel) [RD.15] and HRIC (High-Resolution Imaging Channel) [RD.16][RD.17] are the three optical channels of the Spectrometer and Imagers for MPO BepiColombo Integrated Observatory System (SIMBIO-SYS) suite package [RD.18]. SIMBIO-SYS is the imaging instrument on-board of the BepiColombo mission, ESA Cornerstone n.5, which was launched in October 2018. The mission will reach Mercury by the end of 2025 aiming to a comprehensive exploration of the planet [RD.19].

During the first 6 months of the nominal mission, STC will provide a 3D global mapping with stereo imaging with a minimal spatial resolution of 58 m/px (for details see [RD.2]). The second half of the nominal mission will be dedicated to fill the gaps in the coverage and to observe selected regions through multispectral imaging.

In the first years of the cruise phase several Instrument Check Outs (one every 6 months) were performed to verify the health status of the instrument. The Mercury Composite Spacecraft configuration, with MPO stacked between the Mercury transfer module and the Sun Shield plus MMO, maintains the SIMBIO-SYS channels entrance apertures covered allowing only dark measurements. Only after orbit's insertion at Mercury (after 5 Dec 2025), the instrument's apertures will be free, and the scientific observations will be possible.

2.1. STC STEREO CAMERA

2.1.1. Optical Design and purpose

STC optical design [RD.20] can be divided in two principal components: a double direction optical acquisition system and a common telescope unit (the optical layout is shown in FIG 1).

The double stereo optical system consists in a couple of folding mirrors (see FIG 2) which redirects the $\pm 21.375^\circ$ wide stereo boresight beams along a direction much closer to the system optical axis ($\pm 3.75^\circ$). This configuration increases the magnification ratio of a 0.2% along track direction.

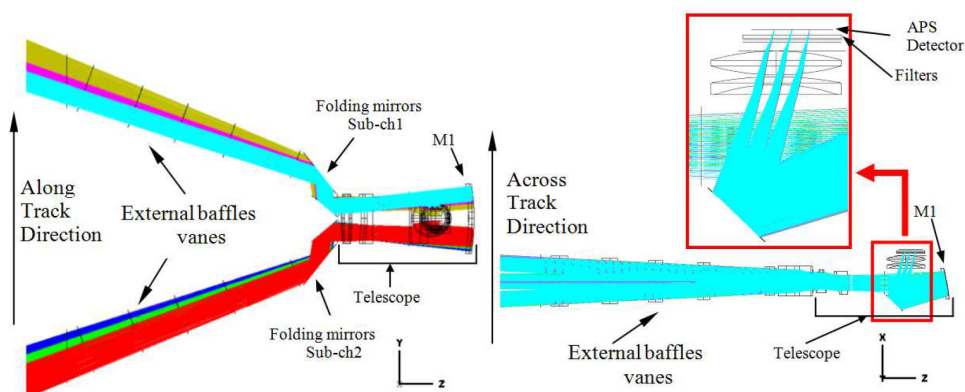


FIG 1 Final overall STC optical layout. In (a) the configuration is viewed in the plane defined by the along track and nadir directions; in (b) the projection in the orthogonal plane, the one including across track and nadir directions, is given. In the inset, an enlarged view of the focal plane region helps to better follow the rays which are focalized on the APS detector.

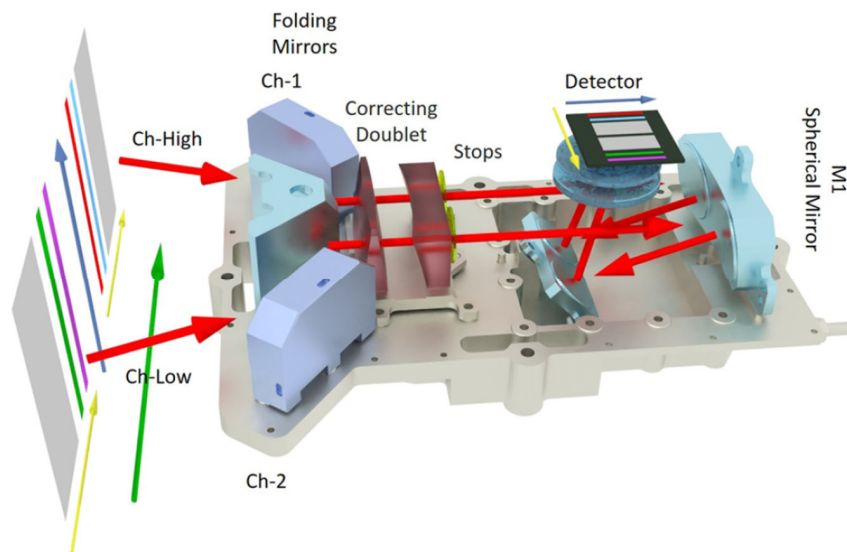


FIG 2 STC 3D optical scheme. The optical path is depicted in red. On the right, the projected on-ground FoV for all the filter frames is depicted. The AT and CT directions are nominally aligned with the detector columns and rows corresponding to the yellow and blue arrows drawn on the detector plane. For more details see [RD.21].

The latter part of the instrument is a modified Schmidt telescope with a focal length of 95 mm. A correcting doublet with null optical power is positioned after the folding mirrors replacing the classical Schmidt correcting plate. The modified configuration reduces the telescope length by about a factor 2 with respect to the classical design.

A common optical path for both sub-channels (Ch-Low and Ch-High in FIG 2) crosses the spherical mirrors and the field correcting doublet focusing on a 10 μm pixel size Si-PIN hybrid CMOS detector (see Section 2.1.2 for details). Different filters are mounted with little separation on the same detector as shown in FIG 3. The detector, described in the next subsection, has a high resistance to radiation and the snapshot image acquisition mode allows a minimum exposure time of 400 ns and permits to acquire images of the Mercury surface maintaining the signal inside the linearity range for the panchromatic filter. The maximum integration time considered for the panchromatic filter during science phase for surface acquisitions is 0.26 ms as derived from the Mercury radiometric model (assumptions can be found in [RD.22]).

5.94°=2016	576px =-2.69°	2.69°=1471px	
	F920		64px= 0.38°
1953 1808			
	F550		64px= 0.38°
1745 1610			
	PANL		384px= 2.30°
1227 820			
	PANH		384px= 2.30°
437 303			
192:319	F420		64px= 0.38°
163 100	240 95		
	F750		64px= 0.38°
(0,0)	32	896px=5.37°	

FIG 3 Diagram shows the definition of the filters on the Focal Strip Assembly (FSA). Start-End-Row column identify the starting and ending rows for each filter (rows included).

Each (sub)-channel aperture stop is placed adjacent to the plano-concave lens of the correcting doublet at a distance corresponding to the focal plane of the M1 mirror (shown in FIG 1). This allows for a good balancing of the aberrations over all the FoV and it guarantees the tele-centricity of the design useful to prevent wavelength shift at the filter strip assembly (FSA).

2.1.2. STC Detector

The STC detector has been developed by Raytheon Vision Systems (RVS) which has produced a custom visible sensor based on a 2048 × 2048 CMOS format [RD.23]. The same device has been employed also for: the SIMBIO-SYS HRIC [RD.17] and a spare model has been mounted on the Colour and Stereo Surface Imaging System (CaSSIS) [RD.24], with photogrammetric purpose [RD.26] for the ExoMars mission. Main detector and ROIC characteristics are reported in **Table 2**.

Geometric		Radiometric	
Parameter	Value	Parameter	Value
Sensor Dimension	2048x2048 px ²	Spectral Flatness	8% (@NIR)
Unit Cell	10x10 μm ²	Mean Quantum Efficiency	92%
Minimum Window Size	64x128 px ²	FPA power budget	120 mW
Max Number of Windows	6	Charge Conversion	14 μV/e-
Integration Time Range	0.4 μs to 5000 ms	Saturation Charge Capacity	120Ke-
Operative Temperature Range	213.5-313.15K	Inverse Gain	7 e-/DN
A/D Conversion	14 bits	Read Out Noise	60e- or 10 DN(@268K)
Fill Factor	100%	Analog Output velocity	<5 Mpps

Table 2 Main detector and ROIC characteristics

The sensor was designed to achieve high sensitivity as well as low readout noise (<100 e-) for space-based, low light conditions. It also must maintain its performance characteristics in a total ionizing dose environment up to 70 kRad (Si) as well as immunity to Single Event Effects, such as latch up and single event upset.

The use of a hybrid configuration allows to benefit from both a high-quality material, especially developed for high quantum efficiency (92%) in a wide spectral range (8% of spectral flatness up to NIR) with a 100% filling factor. A fast and high-performance CMOS ReadOut Integrated Circuit (ROIC) enables an architecture that combines the ability to readout multiple windows through a single analog output, with a power budget of 120 mW. The detector and ROIC are fabricated separately, then bonded together to form a single hybrid structure. **FIG 4** reports the structure of the bonding between the SI-PIN layer and the ROIC.

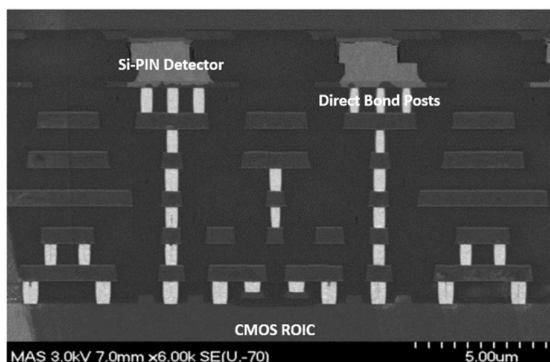


FIG 4 SEM of high-density Direct Bond Interconnect showing, unlike traditional indium bump solution, no air gap between detector and ROIC. In the image five layers of metal can be identified.

Instead of the traditional indium bumps deposited on both the detector and the ROIC to hybridize the two surfaces together, RVS has developed a novel oxide bond interconnect solution with extremely high interconnect yield.

Such a technology has the advantage to leave no air gap between the detector and the ROIC and the bond between the two pieces has less tensions. The tensions can induce bonding breaks if subjected to cyclic thermal gradients.

ROIC basic design incorporates as well an integrate-then read (ITR) operation at the maximum output rate of 5 Mbps. This strategy permits, through the use of the four-transistor unit cell, to perform RESET phase, in which the charge accumulated on the pixel before the acquisition is cleaned, and then to realize the simultaneous integration of photocurrent on all pixels.

No anti-blooming strategy was required for prevention of leaked charge in adjacent pixels, but the detector takes advantage of a reset level control which protects against blooming. The activation of this function is foreseen at 1.2 times the value of Q_{SAT} (see Table 2).

2.2.STC On ground Calibration

The radiometric and geometric responses characterization of the STC channel were accomplished at Leonardo SpA (Florence, Italy) premises.

Most of the calibrations are well reported in [RD.18]; the following sections will give a brief overview of the activities performed on ground:

- from an optical point of view
- Dark Current analysis

Optical calibration

The geometric [RD.21] and radiometric responses [RD.27] of the STC Proto Flight Model (PFM) have been characterized on-ground during the calibration campaigns. The derived responses will be used as a starting point for the calculation of the calibration key data parameters that will be refined with the in-flight calibration.

For the on-ground radiometric calibration (see [RD.3] for details), in order to fully cover the expected radiance range from Mercury surface during the mission, a Labsphere ISS-2000-C Integrating Sphere (IS) has been used (as described in [RD.25]).

The calibration function has been obtained for each pixel of the illuminated regions of the detector because the photo response varies with the region of the CMOS considered. The results consist in the mean slope of the calibration function, which refers to the linearity range of the response curve of the detector. Therefore, the results were applied to calibrate the first set of STC images as described in [RD.27].

The optical distortion [RD.21] has been demonstrated to be very limited (0.3% at the field of view boundary) thanks to the Schmidt design and to the positioning of the aperture stop.

A not common activity [RD.30] was performed at the end of the calibration to validate, in the limited ambient of a clean room, the stereoscopic capability of the instrument.

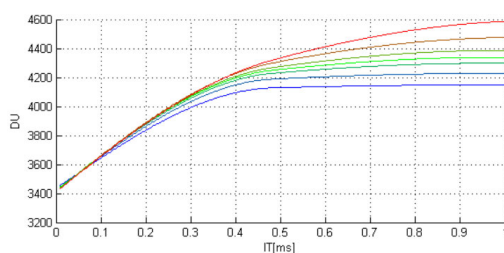
After the on-ground calibration the instrument was mounted on the S/C and operation and planning activities started [RD.31] to reach a complete characterization before the arrival at Mercury.

Dark Calibration

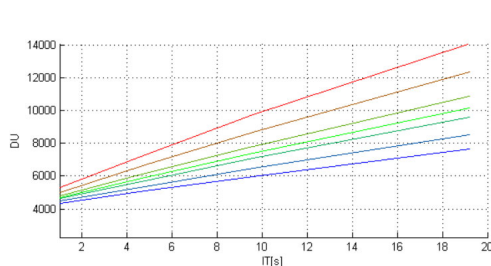
These calibrations performed on the Focal Plane Assembly (FPA) of both the Flight Model (FM) and Flight Spare Model (FS) have the scope to characterize the current generated within pixels in absence of photonic flux. This effect is caused by random generation of electrons due to defects in the depletion region of the photodiode and depends from temperature and integration time. Thanks to these measurements some unexpected effects [RD.32] have been noticed, i.e. charging effects and anomalies into the Dark Signal Non Uniformity (DSNU).

These phenomena can change the response of the detector and they would have reduced the dynamic range of the instrument measurements if not promptly detected and analyzed. Their on-ground characterization will be described in the next session.

The dark current for the STC channel has been measured as a function of the Integration Time (IT) and FPA temperature, as shown in FIG 5. All the acquisitions were commanded with a fixed Repetition Time (RT) (>2s). This parameter allows the ME to command to the PE the acquisitions with a defined time between one image and the subsequent.



(a)



(b)

FIG 5 Dark current trend in Digital Units over the full IT range of the tests shown for short IT=400 ns-1 ms (corresponding to the nominal IT commanded for the GM, panel a) and long IT=1-19.2 s (corresponding to Star Calibration, panel b). In both cases the dark current curves are shown for 7 temperatures of the detector. Middle one (green) represent the nominal temperature 268K, the other ones are separated by 2K between each ones and cover a range with a range between 263K (blue) and 273K (red).

ITs between 400 ns (the minimum IT that can be commanded) and 19.2 s have been used. Temperatures are set in a range of $\pm 5^\circ$ from the nominal operating temperature (268 K).

The DSNU, defined as the standard deviation of a dark image, was measured, and resulted to be limited to 135 DN corresponding to 20.8 mV (considering known the detector's transimpedance and A/D converter response reported in Table 2) for all the dark images acquired for IT lower than 10 ms independently from the temperature. For high integration time (corresponding to 19.2 s) it reaches 61.54 mV.

Read Out noise is limited to 70 e⁻ RMS for low IT and reaches 170 e⁻ for the highest one (corresponding respectively to 10 and 25 DN).

Two detector issues were identified during calibration phase:



Document	BC-SIM-YY-XXX_-_Template		
Date	dd/mm/yyyy		
Issue	1	Revision	0
Page			

- the presence of a “Volcano” region (Section 2.2.1) for a pixel in the detector area not covered by the filters;
- a dependence of the DC from the WT (waiting time or time between two acquisitions) (Section 9) attributable to the Reset capacity of the ROIC.

These two issues are described in the following sections. As demonstrated by the test performed during the Cruise phase, we have developed methods to correct both types of artefacts which will be included into the photometric calibrations pipeline.

2.2.1. Volcano Issue

A “Hot pixels” region has been detected near the panchromatic filters. During the detector calibration, a region of about 9 pixels (outside of the filters regions) resulted to generate blooming effect at nominal temperature (268K) for all the integration times less or equal to 2 ms as shown in FIG 6.

These repeatable phenomena are called “Volcanoes”: when the voltage in the pixel reaches the upper rail, the charge spills over into the neighboring pixels. When these neighboring pixels have enough charge, the spilling further proceeds to their neighbors. The pixels in these clusters are classified as either dead or hot, so their numbers are included in those categories.

However, in the hot pixel volcanoes, historically [RD.33], the signal is not affected by the signal on the neighboring “science” pixels. We are therefore forced to conclude that the event occurs in the bulk of the detector or between the ROIC and detector layer.

During the instrument calibration the team adapted the detector parameters reaching a set of commands (still in use in flight configuration) which will not allow the formation of this effect for nominal acquisitions. **No blooming effect due to the volcano occurred during the measurement of the FPN, DSNU and dark described in the previous section.**

In hindsight, it should be considered that the instrument calibration was always performed with repetition times between the acquisitions near to 2 s.

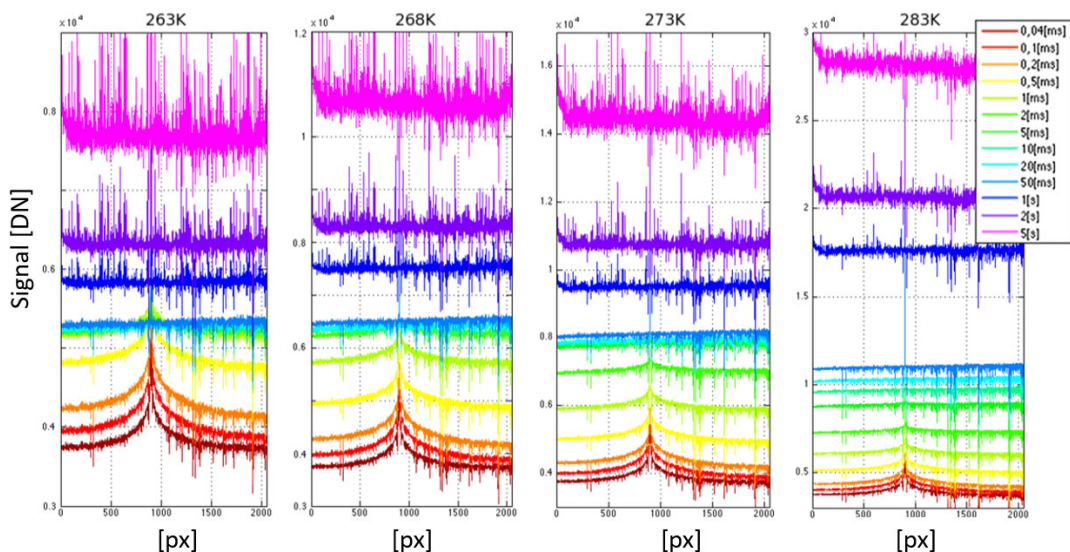


FIG 6 The measurements of the dark current on column 1505 for different temperatures and integration times. Volcano is centered on pixel at column=1505, line=898.

2.2.2. Reset Issue

The FPA calibrations included the measurement of RON, spurious charge and temperature dependence. They highlight another unexpected phenomenon in the detector behavior not correlated with dark or photonic signals but with electronic reset. Since the ITs are limited up to few ms, the DC contribution should be low during FPA calibration. The set of acquisitions performed have demonstrated the presence of a spurious signal of the order of hundreds of DN in the first image of each set. Its value is stabilized during each set of acquisitions. As an example, **FIG 7** shows the evolution of the signal in DN on a reference pixel in the image for 12 set of acquisitions with different increasing ITs; each acquisition is composed by 15 repetitions taken with the same IT (reported in the upper horizontal axis). The sets are separated by a WT greater than the RT. For IT>0.15 ms this effect generates a peak which is absorbed and stabilized in the following acquisitions. Thanks to this test we have demonstrated that the stabilization time depends on the RT.

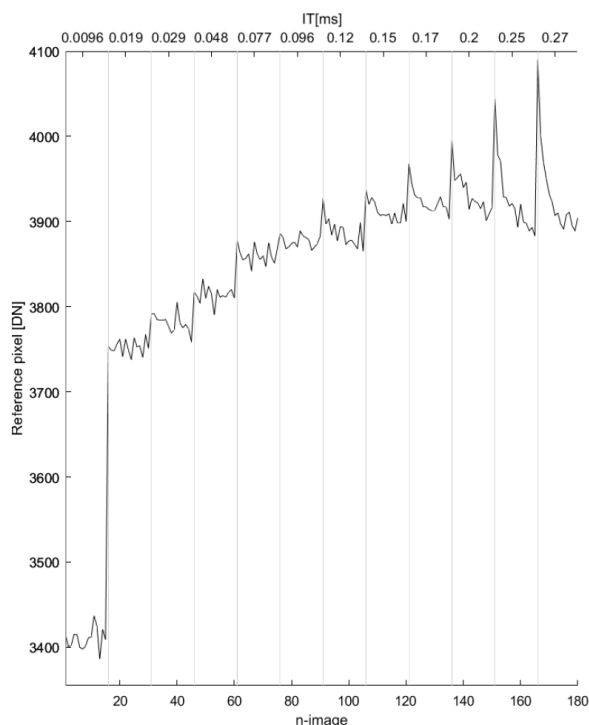


FIG 7 Signal on the reference pixel for sets of images acquired with progressively increased IT. The pixel measured values for 180 images (12 sets) are shown. The IT of each set is reported in the upper X axis and it ranges between 0.0048 ms and 0.27 ms.

Therefore, we can state that at least two different spurious effects are present:

- a Peak Offset (PO) in the DN values of the pixel in the first image of each set (related to the previous waiting time).
- a steep growth of the background signal, named Pedestal Effect (PE), to which DC converges at the end of the sets (related to the RT).

The PE cannot be correlated with DC. DC is, in fact, caused by the statistical transitions of electrons in the conduction band due to thermal energy, and so DC must be linear with integration time. The growth of this background (PE) is steeper, and it seems to reach a saturation level.

It was clear that this effect can be related to the Reset capacity of the detector and probably to its tolerance to the anti-blooming detector strategy.

PO seems to have a different origin. The effect is high but decreases every time a new image is acquired into the same set (same integration time) of the sequence bringing the signal to the Pedestal level.

Such an effect occurs every time a certain time elapses between two images.

The model of this behavior can be described as a dependence of the DC as function of both the IT and RT.

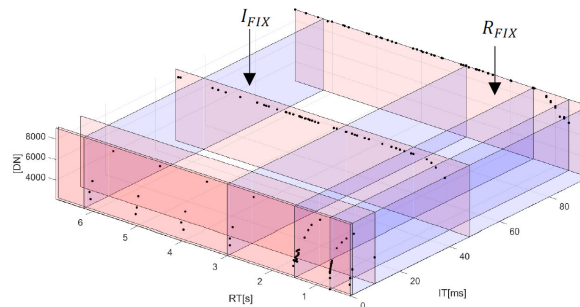


FIG 8 In the picture, the slices in blue represents the curves derived considering the signal dependence only from IT with a fixed RT and vice versa the slices in red represents the signal evolution for a fixed IT at different RTs. The slices defined by a fixed RT are indicated with R_{FIX} , the orthogonal ones with I_{FIX} .

During successive tests, after the instrument has been mounted on BepiColombo S/C and at room temperature 292K, the two different contributions to the signal have been deeper characterized. The PE demonstrates to develop in the first 0.4 ms of the IT. Such a pedestal is not linear with the integration time, but it can be modelled with an exponential function which has a fixed temporal constant (depending on the detector's temperature).

The PO effect is more evident at longer integration times. It builds up during the interval between two images and during the integration time, but it is discharged rapidly during the acquisition of sequences of images with high repetition rate. This charging effect reaches a saturation level for RTs greater than 1.5 s or for ITs <0.5 ms. For these ranges the DC is dependent only by the IT (see **FIG 8**).

2.2.2.1. Reset Issue Solution

Two possible strategies can be adopted to limit or avoid the PO behavior:

- **The Offset Dark Subtraction (ODS)** (always possible but with impact on operations and post processing)
- **The Mitigate strategy** (with impact on the operations)

Offset Dark Subtraction

Considering the tested uniformity of the Peak Offset on the FPA, and thanks to the windowing capabilities of the detector, i.e. 6 different windows can be acquired at the same time, a so called ODS strategy was adopted. The strategy implies the acquisition of a the minimal (64x128 px) region commandable (see **FIG 3**) selected in a not illuminated (and dark coated) area on the detector. It belongs to the regions of the FSA that are black coated to avoid cross-talk between the filter strips. This dark region acquired is called Win-X, it allows to have always a measurement of the PO on the detector and to remove the signal due to the reset effect, and evaluate the effective DC level on the detector.

In FIG 9 the ODS reduction using the Win-X acquisition is described, this method has demonstrated its reliability in the radiometric calibration allowing the calibration of the first set of STC images as reported in details in [RD.27].

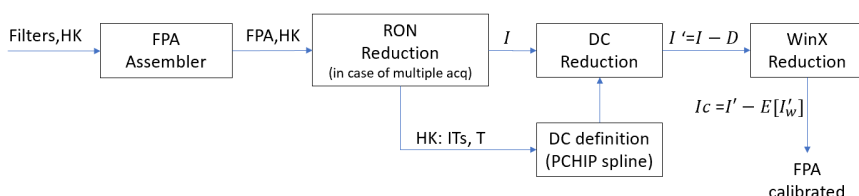


FIG 9 Calibration Pipeline of STC Images taking advantage of the Offset Dark Subtraction of the Reset by the use of the WinX

STC filters images are assembled in the FPA detector. The different windows acquired are inserted at their original positions creating the original FPA matrix representing most of the detector. Then the dark current contribution has to be subtracted. Since the dark current depends on the ITs, and the DC calibration has not been performed at all the possible ITs, the DC values for the considered IT have to be derived via interpolation taking into account the temperature variation. Following the present planning, the interpolation can be performed using the Cubic Hermite Interpolation Polynomial (CHIP)[RD.35].

Furthermore, the ODS has to be performed in order to remove a remaining offset residual (for more details see [RD.27]).

Mitigation

A different strategy (respect the ODS), called “Mitigation”, may constraint the PO to the 1% allowing the full use of the dynamic range. If ODS can be always performed with the limit of increasing the Data Rate of the instrument and reducing the dynamical range without having impact on the accuracy of the calibration, the Mitigate requires the acquisition of additive frames with high RT before the first science acquisition, this means that it will be not possible to adopt this strategy during the GM (where the commanding is based on the Continuous mode). This strategy was demonstrated during ICO4 and is described in this document in Section 3.5.

2.3. OPERATION ACTIVITIES: Flight Operation Procedure

As reported in [RD.2] the two main operative modes of STC are defined as Stereo Mode (SM) and Color Mode (CM).

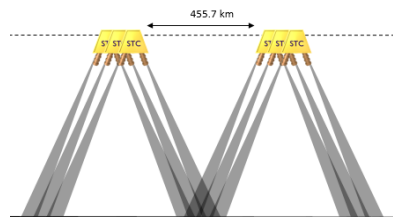


FIG 10 Scheme of the Stereo Mode acquisitions. The mode is defined to perform the global stereo mapping of Mercury surface in the GM phase and the stereo reconstruction of pre-defined targets.

The SM mode (see FIG 10) will be used during the first Global Mapping (GM) phase of the mission to acquire images with Win-X and both the panchromatic filters (or one of them in polar regions) observing all Mercury’s surface in stereo mode.

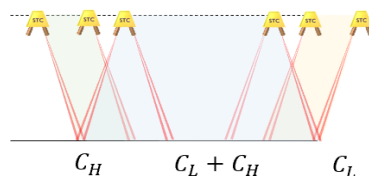


FIG 11 Scheme of the Color Mode acquisitions. This mode is defined to perform Colour acquisitions of pre-defined targets, covering 15% of the Mercury surface. Colour mapping is performed with acquisition of channel C_H and subsequently C_L (or both for great target). The strategy allows to constraint the cross-track and along-track direction according to the defined FoV and geometry.

The CM mode (see FIG 11) is based on target acquisitions with the Win-X and the four color filters (or two of them in the first or last part of the acquisitions).

Both CM or GM are divided in two groups of procedures called “surface” or “stellar” in case of low ITs TCs or high ITs TCs respectively (for details see [RD.4], [RD.5] and [RD.6]). Evaluations, provided by a Spice Kernel [RD.27] based simulator [RD.22] , demonstrated the operations are limited (for surface acquisitions) by a range of Repetition Time and ITs reported in Error! Reference source not found..

Mode	Mean IT [ms]	Max IT [ms]	Min RT [s]	Max RT [s]
Global Mapping	0.1	1.5	5	15
Color	6.4	40	0.8	5


	Document	BC-SIM-YY-XXX_ _Template		
	Date	dd/mm/yyyy		
	Issue	1	Revision	0
	Page			

Table 3 Operative ranges of the ITs and RTs for the two operative modes of STC (Stereo mode for the 2 panchromatic filters and Color Mode for the acquisition of 2 color filters)

Both modes take advantage of the windowing of the CMOS detector. In both cases, the Win-X additive region is acquired to allow spurious effects subtraction by measuring the dark current in the lateral (dark) region of the FPA.



Document	BC-SIM-YY-XXX_ _Template		
Date	dd/mm/yyyy		
Issue	1	Revision	0
Page			

3. CHECK OUTS TIMELINES

After the launch, the SIMBIO-SYS Instrument is periodically monitored to check its health/functionality and to follow the evolution of some key instrument parameters. In the first two years of the cruise there have been: the first instrument test called NECP (Near Earth Commissioning Phase), the delta-Near Earth Commissioning Phase (d-NECP) activity (to complete and repeat some of the NECP ones) and the 4 Instrument Check Outs (performed one every 6 months).

Table 4 reports the different tests performed by STC and the other channels of SIMBIO-SYS after launch.

Name	Date	Duration	Total DV [Gbit]	STC DV [Gbit]
NECP	2018-12-10/12	3d	32.35	18.97
dNECP	2019-06-06	2h 20m	9.2	6.3
ICO1	2019-06-07	4h 21m	8.23	5.9
ICO2	2019-11-27	6h 15m	20.2	8.4
ICO3	2020-06-24	5h 46m	11.58	4.61
ICO4	2020-12-14	5h 42m	3.02	1.16

Table 4 Test Performed after launch with the operation activity duration and the Data Volume (DV) exploited by the SIMBIO-SYS instrument and by the STC Stereo Channel.

Following sections will describe each test in chronological order.



Document	BC-SIM-YY-XXX_ _ Template		
Date	dd/mm/yyyy		
Issue	1	Revision	0
Page			

3.1.NECP and dNECP phase

NECP occurred about 2 months after launch and last 3 days in which the main goal was to measure the DC by means of sets of 10 dark images for 21 different ITs, 2 RTs and different operative modes including the nominal ones, the acquisition of one single filter by times and an orbit simulation (commanding was defined on the SK simulator [RD.22]) to verify the interference with the other channels.

Test analysis is not here reported because was performed at the not nominal temperature of 269K (see [RD.7]) due to a drift of the calibration curve of the set point parameters corrected in the subsequent ICOs. The test was repeated (under the name delta NECP) six months later to avoid this problem (see [RD.8]).

In any case obtained results are in line with the one obtained during the on-ground calibration campaign. Most of the results are reported (at Instrument level) in [RD.34].

3.2.ICO1 phase

During ICO1 a reduced Functional Test was performed and a Performance Test. STC test is reported from an operational point of view in [RD.9]. The Functional Test had the scope of verify the functionality of the instrument in its two acquisition modes while Performance Tests measured the dark for the two operative modes. These tests were repeated with different Repetition Times verifying the effectiveness of the Mitigation Strategy introduced which had the scope of removing the Pedestal Offset depending by the RT and measuring the actual DC on the FPA.

3.2.1. Functional Test

Science data acquired during Functional Test did not present any anomaly. A first reduction of the dataset is shown in FIG 12. The image shows, for each acquisition, the mean value of the windows acquired. Right y-axis (yellow) reports the time between two consecutive acquisitions.

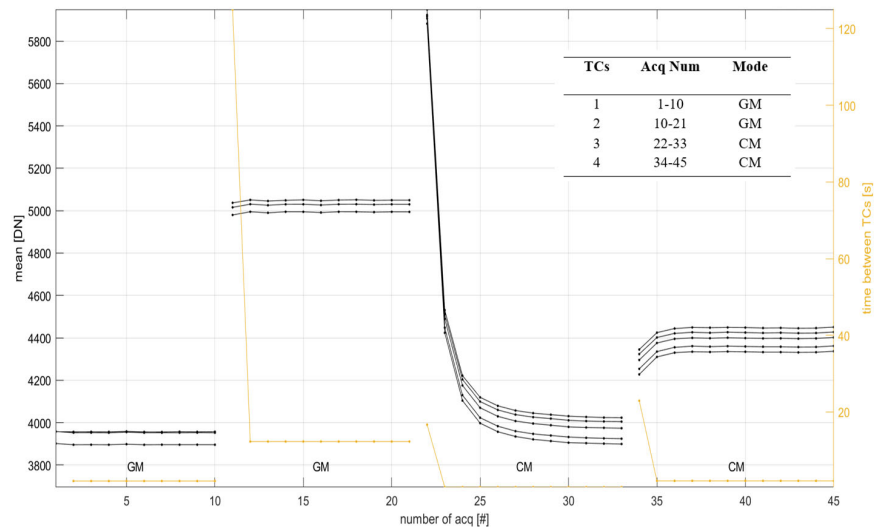



FIG 12 The figure reports the mean of the images of the Functional tests. Each TC command the acquisition of the filters of the mode required always including the Win-X. For example in the case of the first TC , it commands the acquisition of both the panchromatic filters and the win-x. Right y-axis (yellow) reports the time between two acquisitions.

As expected for the GM TCs (commanding ITs of 0.096 ms and 1.5 ms) the signal results nominally constant (within the limits of the RON). In the case of the CM (with ITs of 5.2 and 37.8 ms) the Peak-Offset brought to a not constant level of the dark in the case of long times between the acquisitions as expected. This effect (previously defines as PO) will have no effect during the Scientific Phase of the Mission thanks to the ODS strategy applied with the subtraction of the Win-X from the dark. This approach guarantees to have a correct measurement of the dark both at the beginning or at the end of the acquisition sequences.

	Document	BC-SIM-YY-XXX_ _ Template		
	Date	dd/mm/yyyy		
	Issue	1	Revision	0
	Page			

The drawback is the limitation of the dynamic range of the acquisitions: for this reason an ad hoc operation strategy will be adopted that will be validated during ICO4 (see Section 3.5).

3.2.2. Performance Test Planning

About the Performance Test, as reported in **Table 5**, the two nominal acquisition modes were tested considering two RTs. One nominal and the latter as low as possible:

- in the case of GM, the DC has been measured for minimal RTs (7s) foreseen in the GM phase and for a lower RT (0.45s).
- In the case of CM, the DC was for maximum RTs (5s) foreseen in the CM targeting phase and for a lower RT (0.25s).

These choices can be justified by the necessity to acquire the DC both in nominal configuration (where PO and PE were expected) and in high data rate (where both PO and PE should have less effect) in order to investigate the behavior of the RVS detector for different RT.

Table 5 reports the set of tests acquired during the Instrument Checkout.

Acquisition Mode	IT range	ITs	RT [s]	NAcq
GM	0.4 μ s-9.6s	21	0.45	10
GM	0.4 μ s-9.6s	21	7	10
CM	0.4 μ s-9.6s	21	0.250	10
CM	0.4 μ s-9.6s	21	5	10

Table 5 Acquisitions performed during ICO1 phase. The table reports: the Acquisitions mode used, the number of ITs commanded (corresponding to the number of TCs), the range they spare, the RT commanded (where possible) and the number of acquisitions commanded for each ITs.

The ITs commanded in all cases are 21 but they are not the same between GM and CM: for GM they are concentrated around 0.1 ms while for CM around 6 ms in order to have a better characterization of the DC around the nominally most used operative modes reported in [RD.2]. **Error! Reference source not found.**

3.2.2.1. Performance Test Analysis

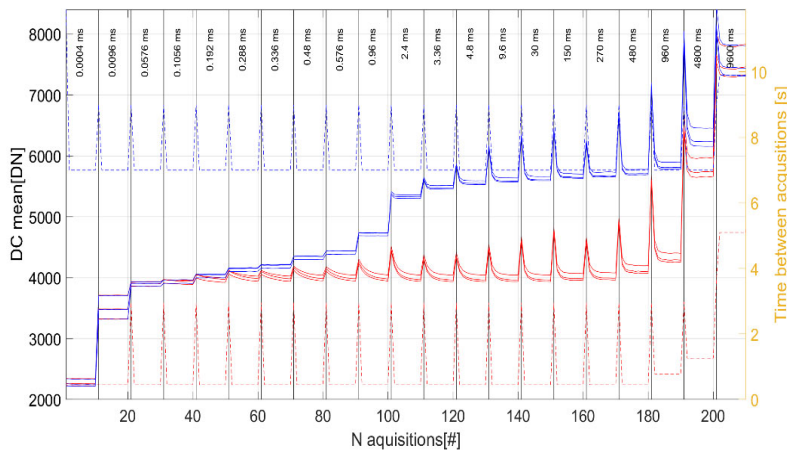
3.2.2.1.1. DC definition

The two GM dark acquisitions sets are represented in **FIG 13** where the means of the windows acquired are shown as a function of the number of the acquisitions. Low RT DC measurements are depicted in red, high RT acquisitions are depicted in blue. In both cases is released the PO while the difference between the two curves can be imputed to the PE.

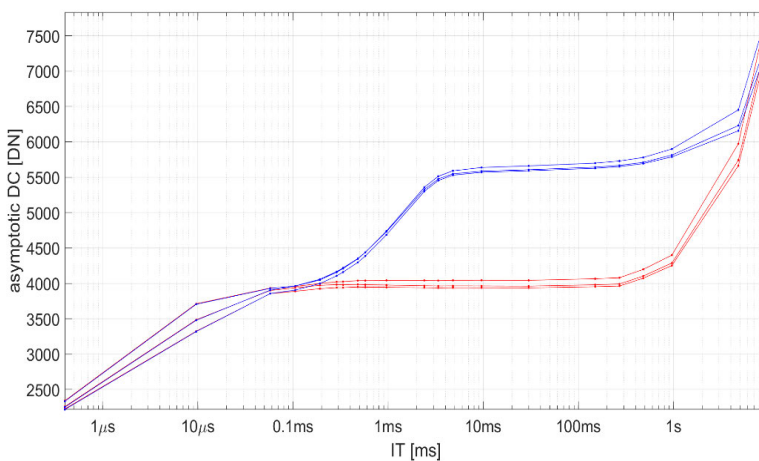
Dotted lines represent the time between each acquisition and previous one (on the right axis).

As expected, high waiting time between two acquisitions increment the DC level. This DC level is then discharged in the following acquisitions.

Each set of 10 acquisitions converges asymptotically to a DC current (depending by IT and RT) which is reported (as average) in **FIG 13** as function of the IT always considering the color red for low RT and blue for high RT.



(a)



(b)

FIG 13 In (a) Mean of the DC for each window acquired (from bottom): window panh e panl. Red lines refer to low RT acquisitions, blue lines refer to high RT acquisition. In both cases dotted lines (with reference to the right y axis) is the waiting time between the images corresponding to 0.45s of RT for red ones and 7s for blue one. Top part of the graph reports for each set of 10 images the IT commanded. For both cases it is evident the presence of the Peak Offset generating the peaks and the Pedestal Effect which generate a difference greater than 1000 DN between the blue and red acquisitions. In (b) Asymptotic mean of the DC for each window acquired (from the bottom): window panh e panl. Red lines refer to low RT acquisitions, blue lines refer to high RT acquisition.

In both acquisition modes the DC increased level was expected to be uniformly on the FPA as demonstrated by on ground calibrations: this makes acceptable the calibration via ODS using the Win-X acquisitions. Unfortunately, as described in 2.2, on ground tests did not consider the RT as a dependence parameter and no test with nominal temperature of the FPA were possible once the instrument was mounted on the MPO.

Comparing the image with low and high RTs acquired during ICO1, the FPA uniformity was not verified.

3.2.2.1.2. FPA not uniformity

Comparing the images with same IT this misalignment results limited to 12 DN (in standard deviation) for most of the surface images and it reaches 30 DN in the case of star acquisition. These values correspond respectively to the 0.3-0.4% of the DC signal. In a limited range around 0.4 ms the standard deviation reached a peak greater than 20 DN (which cannot be justified by the RON) both in the case of the CM and GM.

This preliminary analysis can be well interpreted looking at the next figures (in particular **FIG 14**) where a spatial (not statistic) analysis based on the calibrated images of the PANH and PANL filters is shown.

Considering both benches together (the one with low and the one with high RT): as we demonstrated, a good approach is **to consider the low RT dataset to define the DC and use these images to calibrate the bench of the high RT.**

We can summarize the process by following equations which formalize Calibration Pipeline proposed in **FIG 9**:

$$\underline{I}_{(IT, n_{acq})} = I_{(IT, n_{acq})} - I_{(IT, 10)}^{LOWRT}$$

$$I_{cal}(IT, n_{acq}) = \underline{I}_{(IT, n_{acq})} - E[\underline{WinX}_{(IT, n_{acq})}]$$

The calibration is based on subtracting to each filter image (Win-X included) the reference calibration images (the last for each set of the Low RT acquisitions) and the mean of the Win-X is then removed.

Calibrated images (which should be uniform and showing only the RON noise) are reported in **FIG 14** for the GM ad **FIG 15** for the CM.

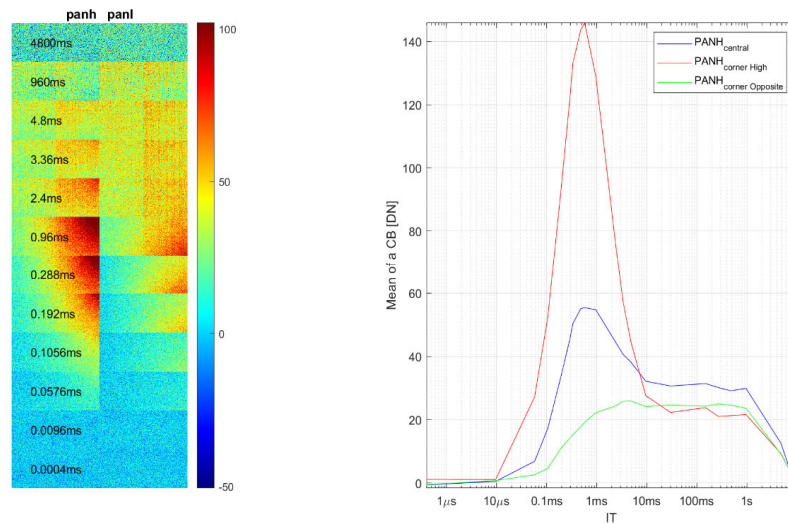


FIG 14 On the left set of images (Panl and Panh) acquired with a RT=7s (the last acquisition for each IT) calibrated (following previous equations) with the set of acquisitions with lower RT (0.45s)(the last acquisition for each IT). Images are overlapped following the IT which is reported in milliseconds. On the right the same calibrated images described by three limited points which represents three regions: In blu the

Compression Box (64x64) centered in the middle of the frame, in red the high one (top-right of the frame), and in green the opposite corner which less. It shows the effect of the blooming

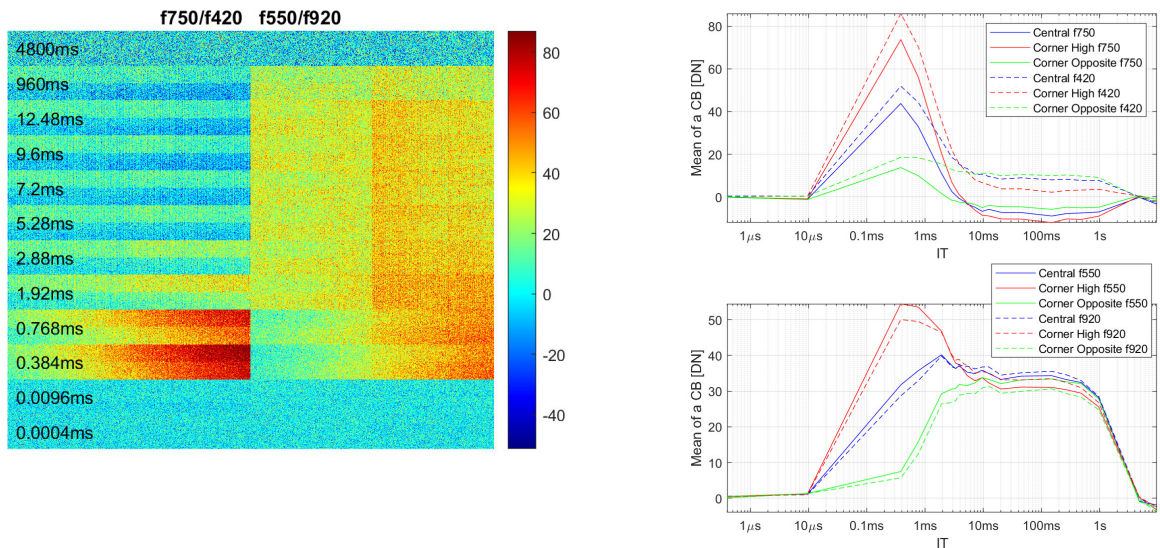


FIG 15 On the left set of images (Channel H and Channel L) acquired with a RT=5s calibrated with the set of acquisitions with lower RT (0.25s). Channel H is shown by overlapping F750 and F420 (left side), Channel L is shown overlapping the other two colour filters. Images are overlapped following the IT which is reported in milliseconds. Colorbar is in DN. On the right the same calibrated images described by three regions: The Compression Box (64x64) centered in the middle of the frame, the high one (top-right of the frame), and the opposite corner. The trends are shown both for Channel H filters (button) and Channel L one (above). It shows the effect of the blooming..

The test demonstrated, as expected, that the assumption that the RT effect can be modelled as a uniform reset level is not always verified but depends by the RT and IT.

In fact, a blooming feature with a peak greater than 100 DN is shown in the PANH filter. For all the last images of each set the blooming is present only for RT=7s and not for RT=0.45s.

The next Instrument Checkout phase (ICO2) was planned to demonstrate that this behavior is repeatable with an accuracy comparable with the readout noise.

The blooming effect starts at 0.1 ms and reaches its peak at 0.576ms (peak correspond to 127 DN corresponding to the 3.17% of the DC signal). For higher ITs the effect becomes lower and can be neglected at 9.6 ms.

Even if CM tests and GM tests were acquired with different sets of ITs, it is possible to assemble the acquired image in manner to have a complete vision of the FPA not limited to the single filters as shown in FIG 16. In the second case it is possible to underline that the source of charge (over the PANH filter) is the Volcano described in Section 2.2.1.

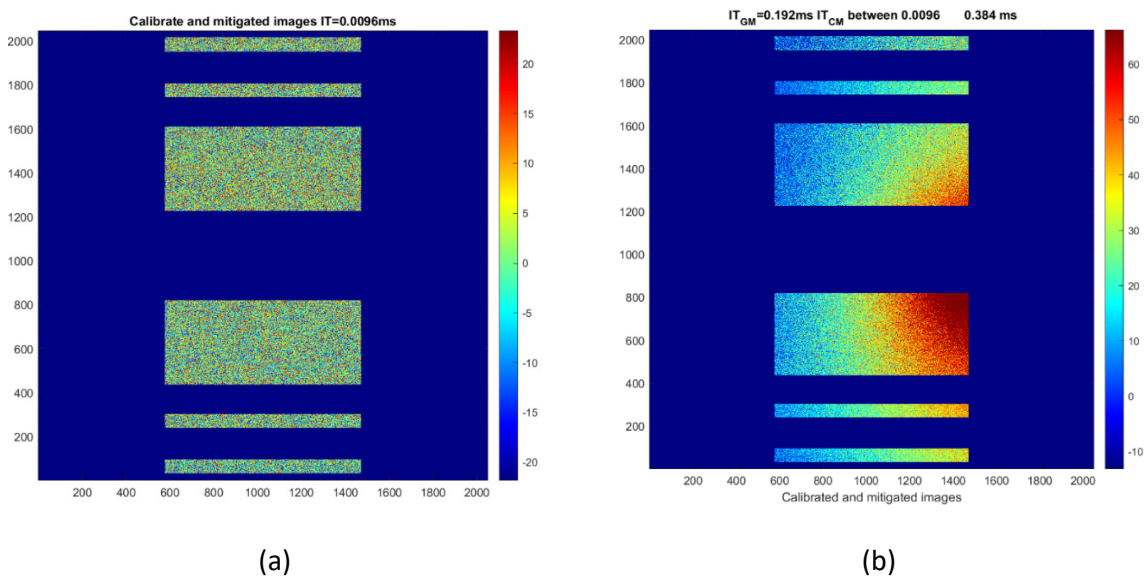


FIG 16 In (a) image assembled of the FPA calibrated and mitigated which correctly shows a std limited by RON (for low IT). In (b) Image assembled of the FPA calibrated and mitigated which correctly shows the effect of blooming for a nominal $IT=3.84ms$

3.2.3. ICO1 Results

The ICO demonstrated the dependence of the DSNU by the Repetition time.

It was clear that the ODS approach adopted in the Calibration Pipeline is still valid but different Calibration Data must be considered as function of the RT. The Calibration Pipeline must be split in two fluxes:

- ones taking account the DC measured for low RTs (without any Volcano evidence),
- the latter based on an additive spurious DC, due to the Volcano, and measured for higher RT.

For this reason, during this ICO, two different sets of acquisitions were acquired both for CM and GM and, in the case of CM the 2 RTs cover the limits of the RT foreseen reported in Error! Reference source not found..

The nominal calibration was bases as:

- a set of images (acquired with different IT) should be considered as reference of the DC (hereafter calibration bench)
- Each new image acquired should be calibrated by subtracting the correspondent image of the calibration bench (if present the IT commanded) or the interpolation of the nearest calibration bench slides (if IT not present).

Following the assumption of this TN the STC calibration should be based on:

- Two calibration benches defined as: one for low and the other for high RT

Document	BC-SIM-YY-XXX_ _Template		
Date	dd/mm/yyyy		
Issue	1	Revision	0
Page			

- **Each new image acquired should be calibrated by subtracting the correspondent image of the calibration bench (each one depending by the commanded RT) or the corresponding interpolation.**
- **The ODS strategy should be applied**

For the GM, the two RTs commanded do not cover the RT range, that will be applied during the scientific operations, planned in the following ICOs. During the ICO4 (see Section 3.5) more dark current measurements have been added to achieve maximal RT of STC (12.3s).

3.3.ICO2 phase

The second Instrument Check out was planned and performed in November 2019 after one year since the BepiColombo launch.

3.3.1. Test Planning

During ICO2 phase different tests were performed:

- The functional test (as in previous ICO)
- the complete dark measurement performed in the ICO1 for the GM mode.
- Large region acquisition of the FPA

The second test had the scope to demonstrate that the measurement performed during the previous ICO was repeatable within the limit of the RON.

The third test had two main goals: firstly to verify the health of the entire detector (even out of the filters regions), furthermore, the part of the detector where the Volcano was detected during on ground calibration was acquired in manner to verify its status in dependence of IT and RT.

More details on all the ICO2 tests are reported in [RD.10].

3.3.2. Test analysis

During the ICO2 it was demonstrated that the dark measurement are repeatable (in the limit of the ROIC).

In addition to these tests during ICO2 large regions of the detector were acquired. As shown in last column of **Table 6** the regions cover the Left, Right and Central bands of the FPA and the upper lower sections(covering half of the FPA). A summary of the acquisitions performed is reported in **Table 6**.

Acquisition Mode	IT range	ITs	RT [s]	NACq	FPA region
GM	0.4 μ s-4.8s	21	0.45	10	
GM	0.4 μ s-4.8s	21	7	10	
Left Band	0.4 μ s, 4.8ms	2	0.7	5	Left
Left Band	0.4 μ s, 4.8ms	2	5	5	
Right Band	0.4 μ s, 4.8ms	2	0.7	5	Right
Right Band	0.4 μ s, 4.8ms	2	5	5	
Central Band	0.4 μ s, 4.8ms	2	1.2	5	Central
Central Band	0.4 μ s, 4.8ms	2	5	5	
Low Part	0.4 μ s, 4.8ms	2	1.2	5	Low
Low Part	0.4 μ s, 4.8ms	2	5	5	
High Part	0.4 μ s, 4.8ms	2	1.2	5	High
High Part	0.4 μ s, 4.8ms	2	5	5	

Table 6 Acquisitions performed during ICO1 phase. The table reports: the Acquisitions mode used, the number of ITs commanded (corresponding to the number of TCs), the range they spare, the RT commanded (where possible) and the number of acquisitions commanded for each ITs.

Right Band, Central Band and Low part (see last column of **Table 6**) of the detector include the Volcanos region which demonstrate to be inactive in all the images with minimal IT of 0.4 μ s. In all the cases with an IT of 4.8ms and RT commanded between 0.7 and 5 seconds the volcanos reached the saturation charge (see **FIG 17**).

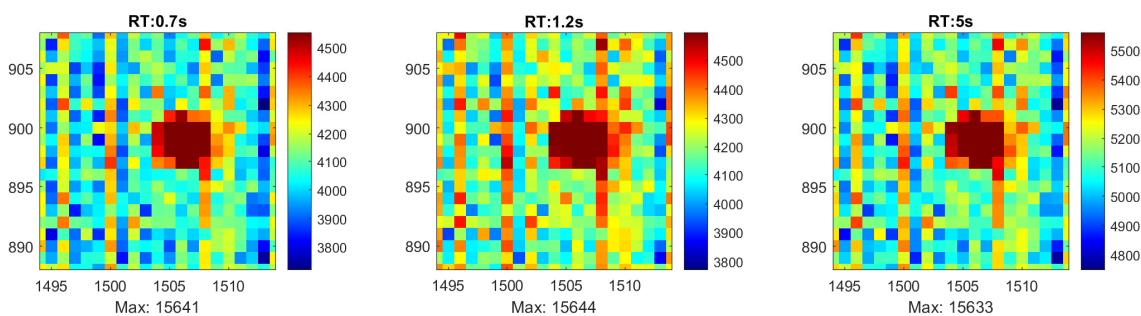
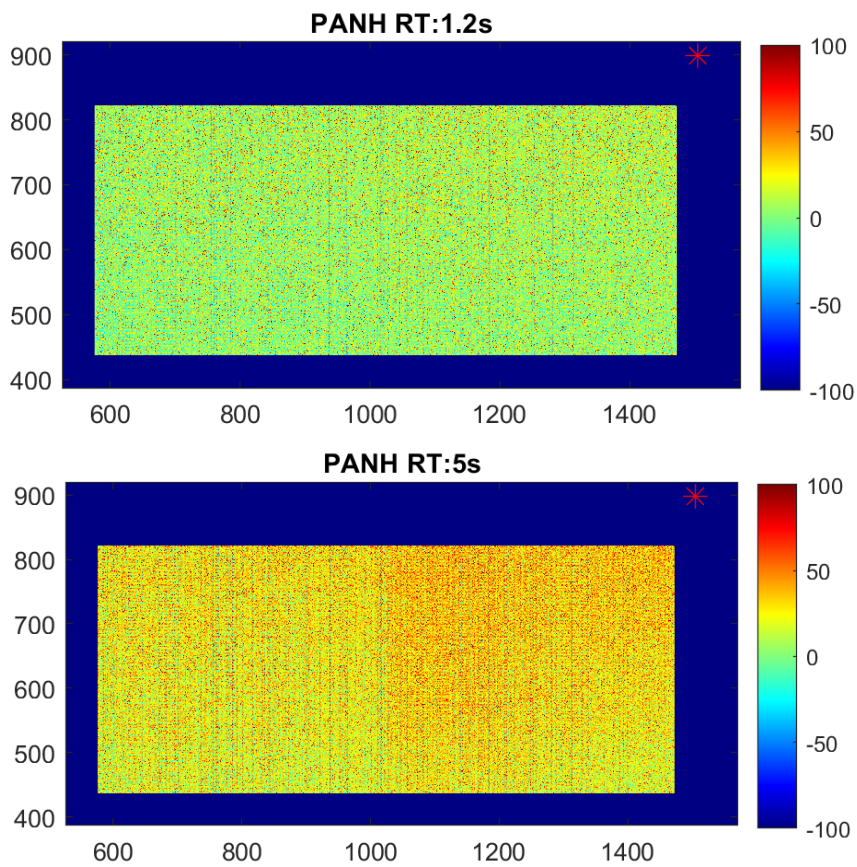
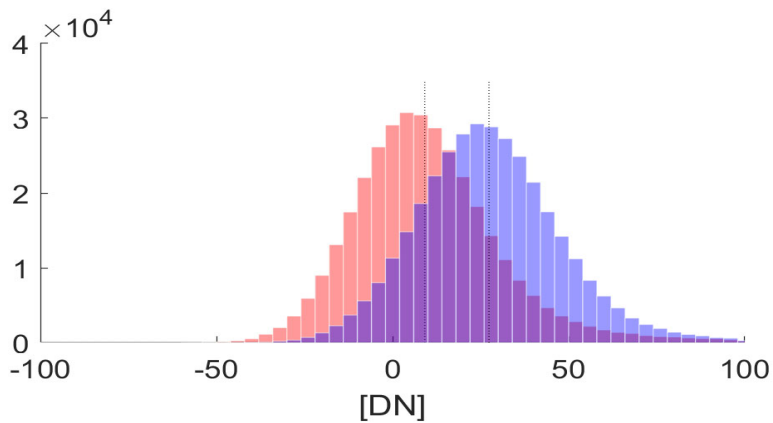


FIG 17 Zoom images of the Volcano region when large part of the detector is acquired with IT of 4.8ms.

Only the Low Part includes in the regions with the high panchromatic filter and the windows X. This means that these images can be calibrated and mitigated with the same bench (without blooming) used in previous ICO.



(a)



(b)

FIG 18 Images acquired during the ICO2 phase in Low Part mode (half of the detector), calibrated with ICO1 images dataset. In (a) the images for the two RT tested; in (b), distributions of the calibrated images. In red the low RT, centered in 0 as expected. In blue the higher RT which presents a 30 DN shift due to the blooming effect.



Document	BC-SIM-YY-XXX_ _ Template		
Date	dd/mm/yyyy		
Issue	1	Revision	0
Page			

The images (see FIG 18) calibrated and mitigated underlining the absence of blooming for low RT (where the distribution has null mean) and a low presence of blooming with a RT=5s.

It is clear that the images acquired in ICO1 with RT=0.25s is coherent with acquisitions with RT=1.2s while the first evidence of blooming appears at 5s which is the upper limit of RT foreseen for Color Mode.

3.3.3. ICO Results

The ICO2 demonstrated the repeatability of the measurement performed in previous ICO. The images, acquiring a great part of the FPA, has **demonstrated the absence of blooming for RT=0.7-1.2s**. In these cases, the DSNU is comparable with the already acquired GM images with RT=0.45s. In all the tests, volcano region reaches the saturation charge for all the ITs, RTs except for minimal IT commandable ($0.4\mu s$).

3.4.ICO3 phase

As described by previous tests both for low (0.45s) of high(7s) RT the images are affected by Peak Offset and in both cases this could be associated to the presence of the blooming on the first images. In both cases the Offset is unloaded by following acquisitions but only in the case of high RT this does not correspond to the blooming removal.

3.4.1. Test Planning

In this section, we propose two examples which makes clearer the phenomena modelling approach applied in all the performed analysis.

Looking at **FIG 13** and **FIG 14** we consider two IT cases:

- the IT=0.288 ms (described in detail in Sections 3.4.2)
- the IT=9.6 ms. (described in detail in Sections 3.4.3)

For both ITs we analyzed:

- a set of images with low RT (0.45s), with a starting Waiting Time (WT) of 2.9 s
- a set of images with high RT (7 s), with a starting Waiting Time (WT) of 9 s

After these examples a generalized analysis for all the ITs will be described in Sections 3.4.4 for GM and Section 3.4.5 for CM.

Image results will be shown in Section **Error! Reference source not found.**

Each pixel DC value can be modelled following an exponential law:

$$DC_V(n) = D_{i,j} + A_{i,j}e^{-n/\tau_{i,j}}$$

Where:

- D is the asymptotic DN signal on the pixels (DC matrix),
- A is the amplitude of the additive signal (due to PO in the mean or blooming in the std) in the first image (Artefact matrix),
- n is the number of subsequent acquisitions
- τ is the hemi life factor (number of acquisitions to be acquired to reach half the additive charge A).

DC is modelled as matrix D with the additive initial spurious sum of the matrix A which is reabsorbed at 50% after a number of acquisitions equal to τ .

All the parameters of this model can be estimated by solving nonlinear least-squares curve fitting [RD.28] on the the parameters for each pixel (the asymptotic DN signal, the Amplitude and the hemilife). Tables 7, 8 and 9 report for the three ITs considered the mean of each parameter on the image, its standard deviation and the mean standard deviation of the model with respect to the measured signal.

3.4.2. Low IT (0.288 ms) Analysis

Parameter	RT=0.45s		RT=7s	
	Mean Value	Std	Mean Value	Std
A [DN]	154.0	26.2	2.2	4.0
τ [#]	4.5	1.2	2.2	3.9
D [DN]	3962.4	128.6	4160.7	134.6
Std Error [DN]	6.8	1.9	8.1	1.98

Table 7 Parameters of the exponential mode for the set of images with IT=0.288 ms for two different RT.

As shown in Table 7 in both cases the model is well describing the measurement because the std of the error model is limited to RON. Dark signal results greater for RT=7s (4160.7 DN) with respect to the RT=0.45 (3962.4 DN) as expected by Pedestal Effect .

A low blooming is present in both cases but:

- for low RT it is discharged after an hemi time of 4.5 acquisitions. Images reach the a standard deviation of the DSNU of 128.6 DN at the end of the acquisitions. At the beginning of the acquisition we can consider and additive disturb with the mean of 154DN and the std of 26.2DN.
- In the case of higher RT, DSNU remains 134.4 (blooming is not discharged)

For low RT it is evident that D represents the DSNU while A is the additive signal introduced by the blooming.

For higher RT the model includes this additive A on D matrices while A is considerable null. The DSNU does not allow an immediate observation of the blooming, that it is clear looking at the calibrated images (FIG 14). The τ parameter shows that the spurious signal has a hemi life of 4.5 acquisitions.


It is clear that in the case of RT=7s no unload is performed during subsequent acquisition. This confirms FIG 13 showing that for IT=0.288 ms the up charging is only linked to low RT.

Same behavior can be observed in the case of IT=0.96 ms.

3.4.3. Higher IT (9.6 ms) Analysis

Different is the FPA reaction for higher IT =9.6 ms and the parameters are reported in Table 8.

Parameter	RT=0.45s		RT=7s	
	Value	Std	Value	Std
A [DN]	507.3	8.7	544.7	8.9
τ [#]	0.9	0.0	0.6	0.0
D [DN]	3969.8	126.2	5588.1	122.8

	Document	BC-SIM-YY-XXX_ _Template		
	Date	dd/mm/yyyy		
	Issue	1	Revision	0
	Page			

Error Model	DN	10.1	2.3	6.7	1.8
-------------	----	------	-----	-----	-----

Table 8 Parameters of the exponential mode for the set of images with IT=9.6 ms for two different RT.

The highest IT has a different behavior. For both RT the DSNU std can be considered the same. In both cases the Artifact std can be neglected: no blooming is underlined but PO is present uniformly on both the RT (the peak reaches a signal greater than 500 DN corresponding to 12.7% of the dark signal).

3.4.4. ICO3 phase: GM analysis

The behaviors reported for the two cases described in previous session can be summarized by

Table 9: low IT allows the generation of the blooming for both RT but is discharged in the case of low RT while remain constant for high RT. For higher IT no blooming is generated but the well-known PO (500 DN) is shown in both cases.

Parameter	RT=0.45s		RT=7s	
	Blooming	Peak-Offset	Blooming	Peak-Offset
IT=0.288 ms	Discharging	NA	Stable	NA
IT = 9.6 ms	NA	Discharging	NA	Discharging

Table 9 FPA Behavior summary observed in case of low and high IT and low and high RT

The same analysis has been performed for all the sets of images with low RT (0.45s) and high RT (7s) for GM. The parameters of the exponential model are shown in **FIG 19** both for low and high RT. **In all the tests the fitting error is lower than RON.**

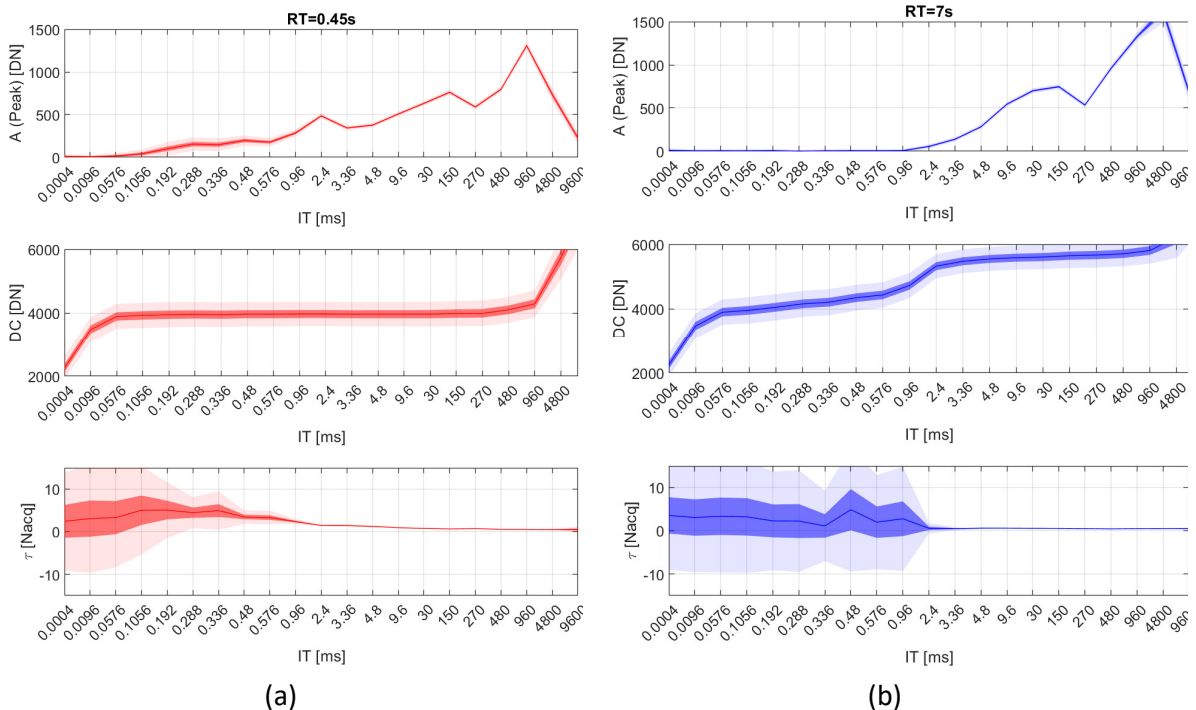


FIG 19 Images show the three parameters A, D, τ for all the IT commanded for low $RT=0.45$ in a and for $RT=7s$ in b.. The plots show the trend, the standard deviation associated (dark red) and 3 times the same value (light red). In a er reported the measurement

In the case of low RT (see FIG 23) the blooming is present only in the first image and it is then discharged in the following one. This phenomenon is true until IT reaches 2.4 ms. The std of the A parameter underlines the presence of the blooming in the first image. When $IT=2.4$ ms this standard deviation is reduced to the RON and the A parameter became uniform on the filter underlining the presence of the PO. The PO is 484 DN for 2.4 ms but can reach 1307 DN for stellar acquisitions these values correspond respectively to the 12 and 24%.

Note that the hemi-lifetime τ is higher in the first part of the test (when the blooming has an effect on the first image). When the blooming is substituted with PO the hemi-lifetime is always less than 1 acquisition.

Dark behavior is very different in the case of high RT (see FIG 24) . The reset in this case is not able to unload the blooming which is not modelled by A parameter but is discharged on the D one which presents a higher standard deviation. Differently by low RT , DC increases with IT. Even in this case the commanding of $IT=2.4$ ms brings to the generation of the PO which reach 1626 DN for stellar mode but fast unloaded by the following acquisition ($\tau < 1$ acq) .

Parameter	RT=0.45s		RT=7s	
	Blooming	Peak-Offset	Blooming	Peak-Offset
$IT < 2.4$ ms	Discharging	Discharging	Stable	NA
$IT > 2.4$ ms	NA	Discharging	NA	Discharging

Table 10 FPA Behavior observed in case of low and high IT and how and high Rt

3.4.5. ICO3 phase: CM analysis

The same analysis was performed for all the sets of images with low RT (0.25s) and high RT (0.5s) for CM. The parameters of the exponential model are shown in FIG 20.

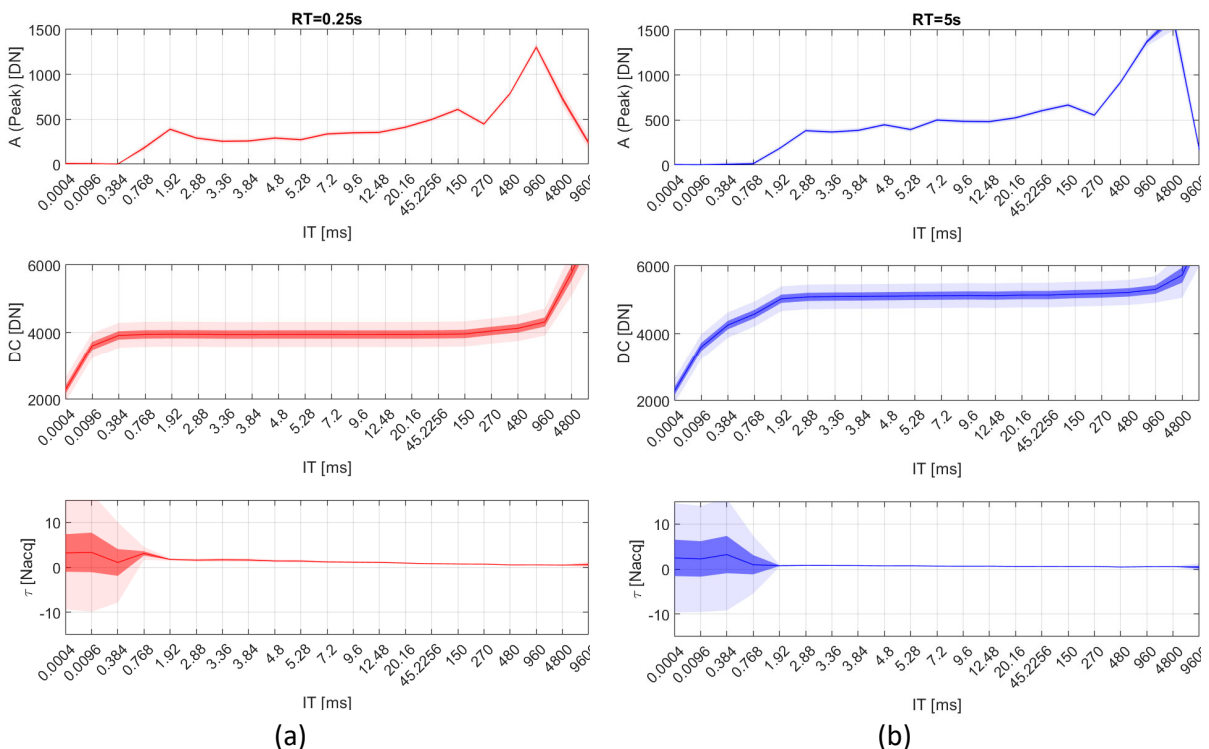


FIG 20 Images show the three parameters A, D, τ for all the IT commanded for low RT = 0.25s in (a) and RT = 5sec in (b). The plots show the trend, the standard deviation associated (dark red) and 3 times the same value (light red).

In case of RT=0.25s an attenuate blooming is visible for IT=0.768ms and IT=1.92ms. It is unloaded in the following acquisitions. For all the greater IT the parameter A models a PO which can reach 1301 DN (corresponding to the 32.52% of the DC signal), as in the GM, in the limited case of IT=960 ms. Same trend can be noted in CM with RT=5 seconds.

3.4.6. ICO3 Results

The Peak Offset has demonstrated to be a consequence of the blooming which invalidate the reset capacity of RVS detector.



Document	BC-SIM-YY-XXX_ _ Template		
Date	dd/mm/yyyy		
Issue	1	Revision	0
Page			

Considering all the test with $RT \leq 5s$ low ITs has demonstrated to generate blooming discharged in the following acquisitions. Higher ITs demonstrated to not generate more blooming but only the Peak Offset which can be automatically mitigated in calibration phase.

$RT=7s$ is the only case in which low ITs generate a blooming which is not discharged by following acquisition but remain stable as part of the DSNU.

The Summary

Table 11 can be now extended to all the cases analyzed during ICO3.

Mode	CM		GM		GM	
	0.25-5s		0.45s		7s	
RT	Blooming	Peak Offset	Blooming	Peak-Offset	Blooming	Peak-Offset
IT<1.92ms	Low and Discharging					
IT<2.4 ms		Discharging	Discharging		Fix	
IT > 2.4 ms		Discharging		Discharging		Discharging

Table 11 FPA Behavior summary observed for all the acquisition modes, RT and IT commanded.

3.5.ICO4 phase

During ICO4 three different tests were performed as reported in

Table 12.

Acquisition Mode	IT range	ITs	RT [s]	NAcq
GM maxRT	0.4 μ s -0.1-5 ms-4.8s	4	12.3	10
Mitigate	0.4 μ s-9.6s	21	7	10

Table 12 *The main parameters implemented during the ICO4.*

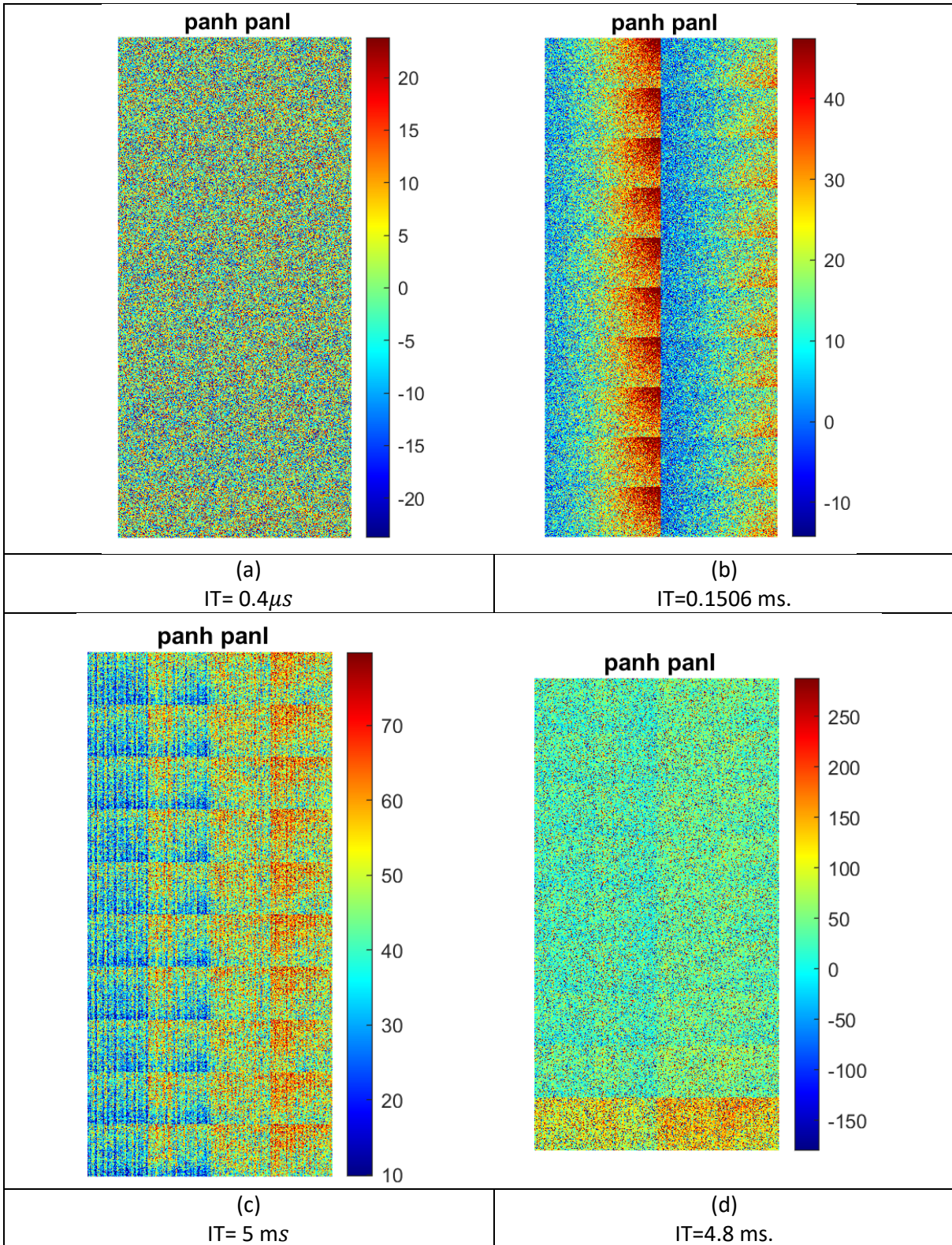
The first test (limited to 4 ITs due to the DV reduction) had the scope to verify the DARK in the GM with the maximum commandable RT (never used in previous ICOs). Second test (Mitigate) was designed to Mitigate and to demonstrate to use in advance the high data rate to avoid peaks in CM acquisitions (as anticipated in Section 2.2.2.1).

3.5.1. GM with max RT

Considering that previous ICOs demonstrated a different behavior between the lower RT and the RT =7s, a set of acquisitions were planned to verify the higher one.

During GM with max RT four sequences of images were acquired (see

Table 12). They were calibrated with the same dataset, the ones previously used as calibration data (RT=0.45s) for example in **FIG 14**. The resulting images (calibrated and offset cleaned by ODS) are shown in the following figures.



Document	BC-SIM-YY-XXX_ _ Template		
Date	dd/mm/yyyy		
Issue	1	Revision	0
Page			

FIG 21 From bottom to top set of images (Panl and Panh) acquired with a $RT=12.3s$ calibrated with the set of acquisitions with lower RT (0.45s)(the last acquisition for each IT). Images are overlapped following the time order. The images are acquired with an $IT= 0.4\mu s$ (a), 0.1506 ms (b) , 5 ms (c) , 4.8 s (d). All images colorbars are in DN

As shown by **FIG 21a** for the minimal IT no blooming is measured and the calibrated and ODS cleaned data correspond to the RON as expected. In all other the blooming is present which is not discharged in the following acquisition.

Same process can be applied using as calibration dataset the images acquired with $RT=7s$ which were affected by blooming. **FIG 28** shows the calibration process results for the first 3 surface TCs which demonstrate in the three cases that blooming at max RT is equal (unless the RON) to $RT=7$ s.

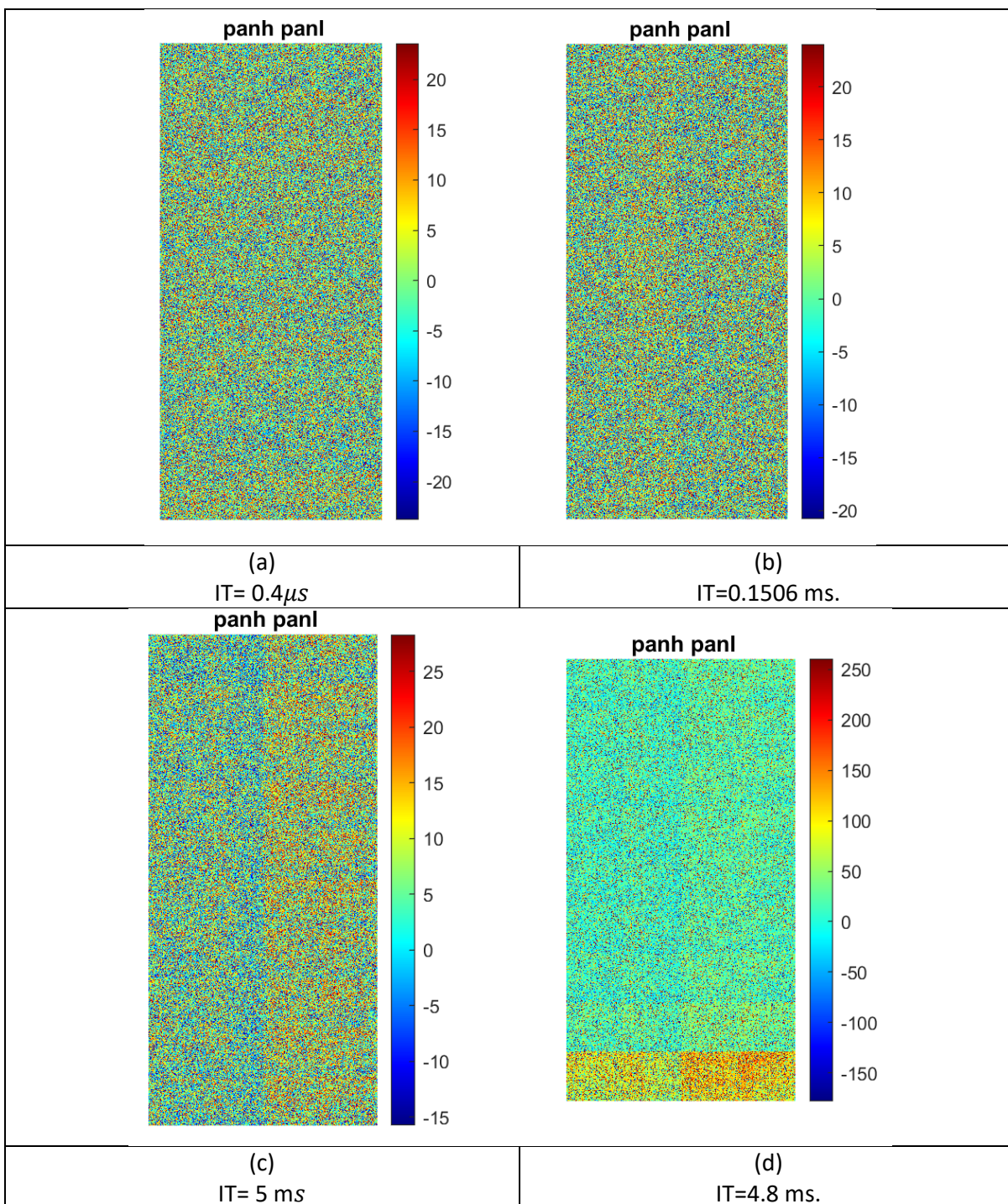


FIG 22 From bottom to top set of images (Panl and Panh) acquired with a RT=12.3s calibrated with the set of acquisitions with lower RT (7s)(the last acquisition for each IT). Images are overlapped following the time order. The images are acquired with an IT= 0.4 μ s (a), 0.1506 ms (b) , 5 ms (c) , 4.8 s (d).All images color bars are in DN.

The calibrated images have a std less than 11 DN (comparable with RON). **This means that the DSNU measured with RT=7s is the same of the one at 12.3 s.**

In the case of stellar acquisitions (TC=4) the std reaches 133 DN (2.2%) for the first image and 103 (1.7%) in the other case while the Peak Offset reaches 91 DN (1.5%) for the first image and 33 DN (0.6%) for the others.

3.5.2. Mitigate test

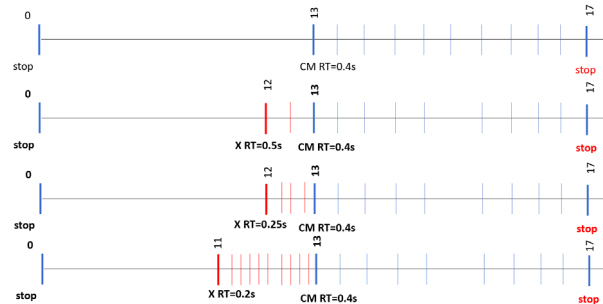


FIG 23 Tests performed during ICO4 to demonstrate the use of pre-use of high data rate to avoid peak in CM acquisitions

The test foreseen four phases:

- in the first a CM with RT=0.4s is executed with a waiting time of 13 s (as performed during functional test) ,
- in the second the CM is anticipated by a Win-X acquisition with RT=0.5s (2 acquisitions) and same IT,
- in the third the RT of the mitigating is brought to 0.25s allowing 4 acquisitions
- in the last Win-X is acquired 10 times with a lowest RT of 0.2 s.

Table 13 reports for each test described (including the functional one) the RT commanded for the TC previous of the CM, the waiting time before the CM sequence, the number of acquisitions performed to mitigate, the mean DC measured in the last frame of the previous TC, the peak measured in the first image of the CM (in DN) and the percentile of the peak reset the functional one (the highest).

Test	Previous TC			CM TC		
	RT	Nacq	Last DC	WT	Peak	Peak perc
	[s]	[#]	[DN]	[s]	[DN]	[%]
FUNC	12.3	#	5068	12.30	5970	100.0
TEST 2	0.5	2	5877	0.50	4233	10.5
TEST 3	0.25	4	5878	0.27	4049	1.0
TEST 4	0.2	10	5766	0.20	3985	-2.2

Table 13 Main parameters and measurements in the Mitigate Test performed during ICO4

The resulting effect of the different strategies on the Peak on the first CM acquisition is shown in FIG 24.

It is important to note that for really high frequency mitigation (TEST4), the RT results to be lower than the one commanded for all the CM acquisitions (0.4s) and the result is a mitigation not only of the Peak Offset but even of the pedestal effect obtaining an increasing DC in the CM acquisition. The test demonstrates that a limited number of acquisitions of Win-X before the CM guarantee to avoid the Peak Effect reducing the DC additive level to the 10% with 2 acquisitions and to the 1% in case of 4.

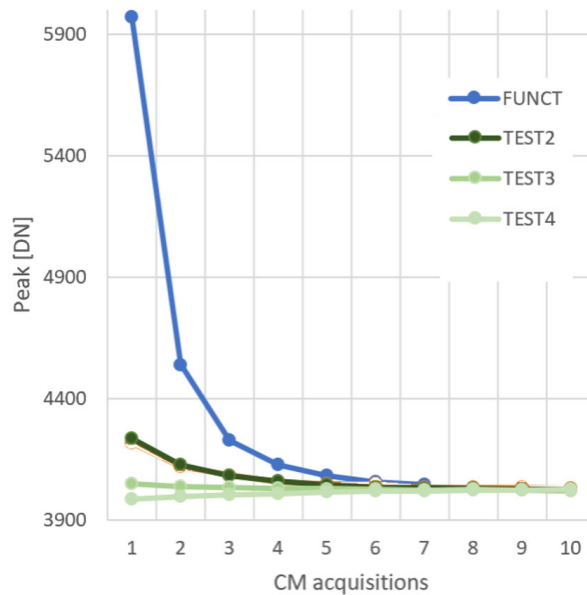


FIG 24 Peak offset measurements. The first image of the CM acquisitions for all the mitigate test performed during ICO4.

3.5.3. ICO4 Results

ICO4 test demonstrates the Mitigate strategy (absorbing the PO and introducing a high rate acquisitions before the one planned).

This strategy will guarantee to use the full dynamic of the instrument during the CM phase. The test demonstrates that a limited number of acquisitions of Win-X before the CM guarantee to avoid the peak effect reducing the DC additive level to the 10% with 2 acquisitions and to the 1% in case of 4.

GM max RT test complete the analysis planned in previous ICOs and gave a complete scenario of the behavior of the instrument.

It is clear that for GM RT (between 7 and 12.3 s) the Blooming effect is fixed and repeatable and can be considered as a typical DSNU.



Document	BC-SIM-YY-XXX_ _Template		
Date	dd/mm/yyyy		
Issue	1	Revision	0
Page			

For lower RT (<5s typical of the CM) Blooming is present only in the first images and is discharged by following acquisitions.

4. CONCLUSIONS

The blooming effect linked to Volcano (2.2.1) and to Peak Offset (2.2.2) were analyzed during the ICOs and their behavior can be summarized by following table:

Mode	CM		GM		GM	
	0.25-5s		0.45s		7s-12.3s	
RT	Blooming	Peak Offset	Blooming	Peak-Offset	Blooming	Peak-Offset
IT<1.92ms	Low and Discharging				Stable	
IT<2.4 ms		Discharging	Discharging		Stable	
IT > 2.4 ms		Discharging		Discharging		Discharging

Table 14 FPA Behavior summary observed for all the acquisition modes, RT and IT commanded.

The tests demonstrated the validity of the proposed Calibration Pipeline considering 2 different calibration dataset images.

- **Nominal Dataset (ND):** acquired (with RT=0.45s in ICO1 (see 3.2) and ICO2 (see 3.3)
- **Blooming Dataset (BD):** acquired (with RT=7s in ICO3 (see 3.4) or 12.3s in ICO4 (see 3.5)

Following Table 14 the Calibration of the STC Images can be summarized by following rules for the two operative modes:

4.1.Global Mapping

In the case of the Nominal GM (see range parameters at Table 3), in which blooming effect is present but is stable and does not depend by the number of acquisitions, the BD dataset can be used as calibration images for the scientific missions.

In the case of a RT<7s and 1.92 ms<IT<2.4 ms (not nominal IT and RT) the blooming effect will have an initial effect on the images but it will be discharged and the ND dataset can be used as calibration images. Same dataset can be used in the remaining configurations.

4.2.Color Mode

In the case of CM the nominal IT is limited between 6.4 ms and 40 ms (see range parameters at Table 3) within this range the blooming has the unique effect to generate the well-known peak which can be calibrated by ODS or avoided by the Mitigation strategy proposed and demonstrated in ICO4 (3.5.2).